Large scale computational screening and experimental discovery of novel materials for high temperature CO$_2$ capture†

Matthew T. Dunstan,[a] Anubhav Jain,[b] Wen Liu,[c] Shyue Ping Ong,[d] Tao Liu,[a] Jeongjae Lee,[a] Kristin A. Persson,[e] Stuart A. Scott,[f] John S. Dennis[g] and Clare P. Grey*[a]

The implementation of large-scale carbon dioxide capture and storage (CCS) is dependent on finding materials that satisfy several different criteria, the most important being minimising the energy load imposed on the power plant to run the process. The most mature CCS technology, amine scrubbing, leads to a loss of 30% of the electrical work output of the power station without capture, which is far too high for widespread deployment. High-temperature CO$_2$ absorption looping has emerged as a technology that has the potential to deliver much lower energy penalties, but further work is needed to find and develop an optimal material. We have developed a combined computational and experimental methodology to predict new materials that should have desirable properties for CCS looping, and then select promising candidates to experimentally validate these predictions. This work not only has discovered novel materials for use in high-temperature CCS looping, but analysis of the entirety of the screening enables greater insights into new design strategies for future development.

Broader context

Given the likelihood of continued fossil fuel use, carbon capture and storage (CCS) technologies become increasingly required, if the world is to reduce atmospheric CO$_2$ concentrations. The current challenge in implementing widespread CCS is finding materials and processes that achieve acceptable levels of energy efficiency. While much work has been done to optimise the processes involved in CCS, less attention has been given to the discovery and optimisation of new materials. In this work we present a high-throughput computational screening methodology that allows the efficient prediction of the relevant CCS properties for known materials, and succeeds in finding several suitable candidates with improved performance over commonly used materials. Furthermore, extensive experimental testing of candidate materials validates the accuracy of the screening and suggests further iterations for its future use.

[a] Department of Chemistry, University of Cambridge, Lensfield Road, Cambridge, CB2 1EW, UK. E-mail: cpg27@cam.ac.uk

[b] Energy Technologies Area, Lawrence Berkeley National Laboratory, 1 Cyclotron Rd, Berkeley, CA 94720, USA

[c] Cambridge Centre for Advanced Research and Education in Singapore, Nanyang Technological University, 1 Create Way, Singapore 138602, Singapore

[d] Department of NanoEngineering, University of California San Diego, 9500 Gilman Drive, Mail Code 0448, La Jolla, California 92093-0448, USA

[e] Department of Materials Science and Engineering, University of California Berkeley, 210 Hearst Mining Building, Berkeley, CA 94720, USA

[f] Department of Engineering, University of Cambridge, Trumpington Street, Cambridge CB2 1PZ, UK

[g] Department of Chemical Engineering and Biotechnology, University of Cambridge, Pembroke Street, Cambridge, CB2 3RA, UK

† Electronic supplementary information (ESI) available. See DOI: 10.1039/c5ee03253a

Introduction

The challenge of reducing anthropogenic greenhouse gas emissions, particularly that of CO$_2$, has been the focus of numerous governmental and industrial initiatives in recent years. Despite government policies penalising industry for CO$_2$ emissions, it is likely that total global emissions of CO$_2$ will continue to increase over the next decades as countries continue to exploit their natural resource reserves.[1] In this instance, large-scale carbon dioxide capture and storage (CCS) applications represent one of the main initiatives to mitigate the rise of global CO$_2$ emissions.[2]

There are a number of different broad categories of proposed materials to separate CO$_2$ from the flue gas mixture, typically composed of ~75% N$_2$, ~10–15% CO$_2$, ~10% H$_2$O, and ~3% O$_2$ at 40 °C and 1 atm. These include physical adsorption

1346 | *Energy Environ. Sci.*, 2016, **9**, 1346–1360

This journal is © The Royal Society of Chemistry 2016

processes utilising materials with high internal surface areas such as zeolites, metal–organic frameworks (MOFs), zeolitic imidazolate frameworks (ZIFs) and activated carbons;[3–6] physical separation processes utilising membrane materials[7] and high temperature CO_2 absorption looping processes involving the chemical reaction of CO_2 with alkaline earth oxides, notably MgO and CaO and related materials to form solid carbonates.[8] These high-temperature processes are particularly appealing, given the possibilities of achieving very low energy penalties (∼6–8% with respect to reference power plants without CO_2 capture), the maturity of the technology being reflected in the number of pilot plants using CaO-based sorbents already operating around the world, and the wide range of materials that could possibly be used in such a process.[9]

There is interest in developing new materials for high-temperature CCS, or modifying existing ones, because of the problems with capacity loss encountered when using a pure CaO–$CaCO_3$ system. In studies using natural limestone, the CO_2 capture capacity of the solid sorbent can decrease by as much as 90 mol% within 5 cycles owing to sintering of the solid particles.[10] Recent research has focussed on the use of various additives to form solid supports and avoid sintering of the limestone, including Al_2O_3, $Ca_{12}Al_{14}O_{33}$, SiO_2 and MgO.[11–13]

Beyond the current approaches, there is a very wide range of basic oxide materials which could potentially be used in developing an optimal process. Practically, synthesising and testing all possible materials is not feasible, and therefore it is desirable to develop a screening methodology based on *ab initio* computations to identify the most promising candidates for the target application.

There have been a few examples of previous approaches utilising various theoretical methods to screen materials for CO_2 capture. Lin *et al.* generated a database of potential zeolite-like structures that were subsequently analysed *via* interatomic potentials to determine their thermodynamic stability.[14] CO_2 absorption isotherms were constructed using molecular simulations, which allowed the calculation of the parasitic energy for the stable materials, corresponding to the penalty imposed on a power plant if fitted with a CCS process using the material (including the energy to compress the gaseous CO_2 for storage). Their screening showed a theoretical limit to the minimum parasitic energy obtainable with zeolitic and zeolitic imidazolate framework (ZIF) materials. A subsequent study applied this parasitic energy metric to a wider class of materials including both experimentally-realised and hypothetical materials, finding that it is suitable for evaluating materials for CCS, as it combines various relevant thermodynamic properties.[15] Several other studies have also been performed on similar materials, albeit on small sets, with some comparison between theoretical and experimental results.[16–18] High-throughput synthesis methods have also been used to find novel ZIF materials for CO_2 capture.[6]

The group of Duan *et al.*[19–21] have focussed on lithium-based oxide materials for high-temperature CCS applications, using density functional theory (DFT) and phonon calculations to determine the carbonation reaction thermodynamics of these materials, and comparing them with experimental results.

Other studies have also outlined a possible screening process based on theoretical DFT and phonon calculations to identify the most suitable materials from a large starting set, with screening performed on smaller sets of alkali-based oxides.[22,23] The limitation of these studies is that they were applied to a relatively small number of materials, many of them already well known experimentally as being promising compounds for CO_2 capture.

The goal of the present study is to theoretically screen thousands of possible carbonation reactions from a very wide range of solid oxide based materials, both with the hope of discovering novel compounds for CCS applications, and that the screening results can help elucidate the underlying principles that can drive future design of CCS materials. Thus, we have utilised the Materials Project database (www.materialsproject.org), which contains structural, electronic and energetic data for over 50 000 compounds (as of August 2014) calculated using the Vienna *Ab initio* Simulation Package (VASP).[24–26] Importantly, the contents of the database are accessible *via* the REST Materials API,[27] which allows users to develop their own screening programs to search the database using an open-source Python library (pymatgen) for materials analysis.[28] In this work, a screening methodology was developed to search the database for suitable materials for high-temperature CO_2 capture and to predict the thermodynamic enthalpies for the *in silico* carbonation reactions of these compounds. To rank these reactions we used an energy penalty concept as used by others,[14] which favours materials whose use for CCS minimises the energy load imposed on a power station. We also screened materials based on their gravimetric CO_2 capacity as a preliminary measure of the material cost per unit of CO_2 captured, and also the net volume change of a material after carbonation as an indication of cycling stability.

Experimental investigations of the carbonation reaction thermodynamics, cycling stability and morphological changes were performed as a comparison to the theoretical predictions, so as to go beyond the solely theoretical framework used in previous studies. X-ray diffraction (XRD) was used to characterise the structures of the materials both pre- and post-reaction, thermogravimetry and differential scanning calorimetry (DSC) was used to characterise the carbonation enthalpy and cycling capacity, while scanning electron microscopy (SEM) allowed us to characterise the changing surface morphology of the cycled materials. The particular candidate materials were chosen for a number of different reasons. Firstly, materials for which there had been no previous CO_2 capture properties reported were studied to validate the claim that the screening could suggest truly novel materials for CCS applications. Other materials were then selected either as (i) benchmark materials to provide as wide a comparison with other studies, or (ii) because of their predicted performance as CCS materials. The experimental studies showed that the theoretical screening could indeed accurately predict (within error) the carbonation properties of the candidate compounds, validating this method as a tool for the discovery of novel CCS materials. Furthermore, rational design guidelines emerged from the overall screening results,

This journal is © The Royal Society of Chemistry 2016

Energy Environ. Sci., 2016, 9, 1346–1360 | **1347**

giving valuable insights as to where future research efforts should be aimed to optimise the materials used in CCS.

Methodology

Dataset construction

Given the ground state energies of all the phases present in a given carbonation reaction, it is possible to calculate ΔE_{DFT} for the reaction, which is equal to $\Delta H_{carbonation}$ at 0 K and zero pressure. The first part of the screening process therefore is to determine this value for all possible reactions within a given subset of compounds. Furthermore, since these reactions will be performed at varying CO_2 partial pressures and temperatures, a single variable can be defined by considering all reactions under varying CO_2 chemical potential (μ_{CO_2}), with a more negative value corresponding to either higher T or lower p_{CO_2}.

The screening focussed on oxide materials that were either binary or ternary compounds in this initial screening, as this not only drastically narrows the phase space within which the search is conducted, but it also excludes compounds with four or more elements that are more likely to phase segregate to simpler binary or ternary compounds during the cycles of carbonation and calcination. Furthermore, materials were limited to those containing elements from the 37 most abundant within the earth's crust, because this realistically reflects concerns about cost and availability of a useful CCS material.‡ The geometry optimised structures and ground state E_{DFT} of the relevant materials were retrieved from the Materials Project database, having been previously calculated by the Materials Project using VASP.[24]

The screening comprised 640 unique compounds with a total of 1442 simulated carbonation reactions. To obtain all compounds that matched these initial criteria, quaternary phase diagrams of the form A–M–O–CO_2 were simulated, where M is a non-alkali element, using the Phase Diagram app within the pymatgen library.[30,31] Because the primary interest lies in the evolution of the phases under reaction with CO_2, the approach found in previous studies that generated open phase diagrams with respect to μ_{O_2}[31,32] was adapted to study the phase equilbria under changing μ_{CO_2}.

Open phase diagram construction

In order to construct these phase diagrams, we initially assumed that the system is closed with respect to every element except CO_2, which is non-ideal but reasonable given that $p_{CO_2} > p_{O_2}$ during both the carbonation and decomposition reactions. Furthermore, we separately tested each compound for its stability with respect to p_{O_2}, and this was included as an additional filter in our screening, excluding compounds that would oxidise or reduce under conditions similar to those for carbonation. In this case the relevant potential is the CO_2 grand canonical potential which can be defined as:

$$\phi(T, P, N_A, N_M, N_O, \mu_{CO_2}) = G - \mu_{CO_2}N_{CO_2} = E - TS + PV - \mu_{CO_2}N_{CO_2} \tag{1}$$

where G is the Gibbs free energy, E is the internal energy, T is the temperature, S is the entropy, P is the pressure, V is the volume, and N_i is the number of atoms of species i in the system. If it is assumed that the change in the PV term is small and primarily cancels between the solid phases relative to the E and TS terms for a reaction that primarily involves solid condensed phases, and ϕ is normalised so that the sum of the A, M and O components is equal to 1, eqn (1) can be rewritten as

$$\phi(T, P, x_A, x_M, x_{O_2}, \mu_{CO_2}) \approx \frac{E - TS - \mu_{CO_2}N_{CO_2}}{N_A + N_M + N_O} \tag{2}$$

where x_i is the component fraction of i in the ternary phase diagram. To clarify, N_O is the amount of oxygen remaining in a phase after adding or removing stoichiometric amounts of CO_2, for example in the phase Li_2CO_3, $N_{CO_2} = 1$ and $N_O = 1$.

In order to construct these open phase diagrams it is normally necessary to calculate the entropy change in the solid and gas phases due to different vibrational, configurational and electronic excitations. For solid crystalline structures this would normally be approached by calculating the various phonon frequencies (and hence the phonon densities and dispersion curves) for individual phases and using these to derive the total vibrational energy of the crystal at different temperatures. This approach is tractable when it comes to studying a small number of phases and reactions, but in a screening study involving thousands of different compounds, these calculations are too expensive to be feasible.

Fortunately, some assumptions can be employed to simplify the calculation of the phase diagram. Given that all the reactions of interest involve CO_2 gas absorption, it is reasonable to assume that the reaction entropy is dominated by the CO_2 gas entropy, rather than changes due to solid–solid transformations. In fact, it has been previously shown that the Gibbs free energy of solid phase surfaces vary to a very small degree (<10 meV) over a wide range of temperatures (<1500 K) and pressures (<100 atm).[33,34] As such, the change in the CO_2 chemical potential can account for the majority of the effect of temperature on ϕ. At a given temperature T and CO_2 partial pressure p_{CO_2}, the chemical potential can be described as:

$$\mu_{CO_2}(T, p_{CO_2}) = E_{CO_2} + PV - TS_{CO_2}^{T,p_0} + kT \ln \frac{p_{CO_2}}{p_0} \tag{3}$$

where p_{CO_2} is the CO_2 partial pressure, p_0 is a reference CO_2 partial pressure (0.1 MPa), k is Boltzmann's constant and $S_{CO_2}^{T,p_0}$ is the CO_2 entropy, obtained from the NIST-JANAF thermochemical tables.[35] If the gas is ideal, the PV term is equal to kT, leaving the chemical potential dependent only on T and p_{CO_2}. The expression for ϕ can be further simplified, given the assumption that the contribution of S_{CO_2} within $\mu_{CO_2}N_{CO_2}$ dominates compared to S (the entropy of the solid phases):

$$\phi(T, P, x_A, x_M, x_{O_2}, \mu_{CO_2}) \approx \frac{E - \mu_{CO_2}N_{CO_2}}{N_A + N_M + N_O} \tag{4}$$

It is possible then to interpret carbonation reactions as the evolution of phases over successive ternary phase diagrams A–M–O with different μ_{CO_2}, essentially tracking the decomposition
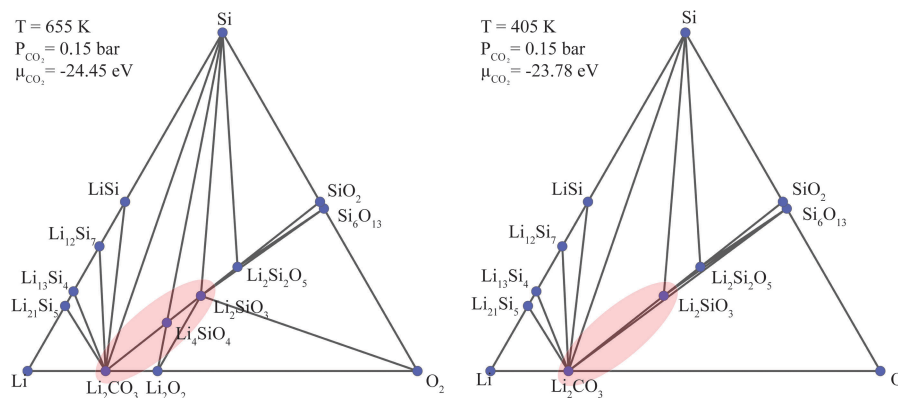
---

‡ Sb was also included in the screening, despite not being within the most abundant elements, because of our work on a novel CCS material, $Ba_4Sb_2O_9$.[29]

1348 | Energy Environ. Sci., 2016, 9, 1346–1360

This journal is © The Royal Society of Chemistry 2016

Fig. 1 Ternary Li–Si–O phase diagrams under different μ_{CO_2} obtained by applying the CO_2 grand potential to the Materials Project database. The physical equivalent of increasing the chemical potential is either an isothermal reaction performed with increasing p_{CO_2}, or an isobaric reaction under decreasing temperature. Vertices that are present in the lefthand phase diagram but are not present in righthand phase diagram represent phases which have decomposed as a result of the change in μ_{CO_2}. The product phases of this decomposition reaction with CO_2 are situated at the vertices at either end of the edge where the original phase was formerly located. For example, Li_4SiO_4 transforms to a mixture of Li_2CO_3 and Li_2SiO_3 with increasing μ_{CO_2} (see pink shaded area of the phase diagram).

of a given phase under increasing temperature or CO_2 partial pressure. An example of this can be seen in Fig. 1, showing different projections of the Li–Si–O–CO_2 phase space at constant μ_{CO_2} slices.

A summary of the assumptions used in simplifying the CO_2 grand canonical potential can be seen in Table 1.

Correction for CO_2 molecule

It is also necessary to obtain a more accurate estimation of the energy of the CO_2 molecule found in the database, because the database entry for CO_2 is based on solid, rather than gaseous CO_2. More pertinently, solid–gas reactions in density functional theory are subject to non-cancellation of errors that often require empirical adjustment.[36,37] To this end we calibrated the database energy by comparing ΔE_{DFT} and $\Delta H_{experimental}$ at 293 K for a small set of basic binary alkali oxides, and a number of ternary Li-based oxides (Fig. 2). The average error between the theoretical and experimental values was added as a correction to E_{CO_2}, and the corrected value was used for the screening. This correction will also account for some part of the solid entropy change between 0 and 293 K not taken into account in the calculations.

Comparison to other theoretical studies

There are previous theoretical results derived from a similar level of DFT theory to model ΔE_{DFT} for the carbonation

reactions of binary oxides and some different reaction pathways for Li-based ternary oxides.[19,20,23,38] To validate the calculated energies in the Materials Project database, we compiled these previous results and compared the respective ΔE_{DFT} for the various reactions. The respective values for ΔE_{DFT} are shown in Fig. 3.

It can be clearly seen that there is a small but constant overestimation (more negative) of ΔE_{DFT} in this work compared to the previous studies. The main source of deviation between the two studies is the different values of E_{CO_2} used: -2191 kJ mol^{-1} and -2219 kJ mol^{-1} for our study and the work of Duan *et al.* respectively,[22] which would lead to our more negative ΔE_{DFT}.

Energy penalty calculations

To evaluate the potential use of these compounds in CCS applications, the overall parasitic energy penalty that would be imposed on a model power plant through the use of this material was considered, following the approach in previous studies.[14] Further details of these calculations are available in the ESI.†

Synthesis of candidate materials

Pure polycrystalline samples of the candidate materials were prepared using a solid-state method. The starting reagents and synthesis conditions are summarised in Table 2. Prior to weighing, $CaCO_3$ was dried at 1000 K overnight to ensure there was as little moisture present in the compound as possible.

Table 1 The form of the CO_2 grand canonical potential, and the assumptions used to obtain the simplified expressions used in the screening

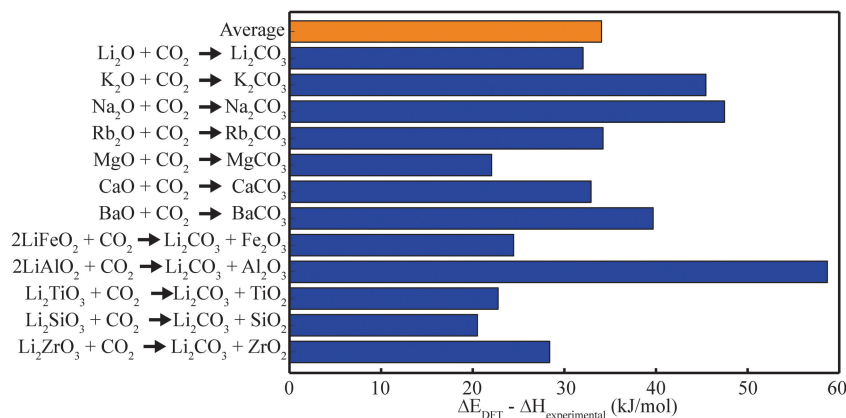| ϕ	Assumptions
$E - TS + PV - \mu_{CO_2}N_{CO_2}$	Exact form
$E - TS - \mu_{CO_2}N_{CO_2}$	PV small relative to $E - TS$
$E - \mu_{CO_2}N_{CO_2}$	S small relative to S_{CO_2} (contained within μ_{CO_2})
$E - N_{CO_2}\left(E_{CO_2} + kT - TS_{CO_2}^{T,p_0} + kT\ln\dfrac{p_{CO_2}}{p_0}\right)$	CO_2 behaves as an ideal gas
$E^{DFT} - N_{CO_2}\left(E_{CO_2}^{corr} + kT - TS_{CO_2}^{T,p_0} + kT\ln\dfrac{p_{CO_2}}{p_0}\right)$	$E = E^{DFT}$ at 0 K, E_{CO_2} fitted to experimental values

Fig. 2 Errors between ΔE_{DFT} and $\Delta H_{experimental}$ at 293 K for selected binary and ternary oxides. The average error was used as a correction to E_{CO_2} in the Materials Project database.
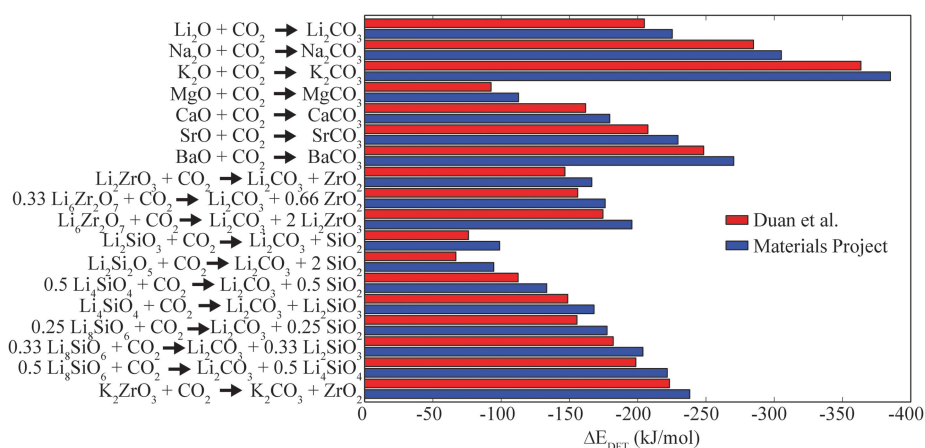

Fig. 3 Comparison between the calculated ΔE_{DFT} for this work (blue), and with the studies of Duan et al. (red).[19,20,23,38] There is a small but constant difference between the two studies, with the Materials Project ΔE_{DFT} being 21 kJ $mol_{CO_2}^{-1}$ lower than the previous study on average.

Table 2 Synthesis conditions and starting materials for the compounds in the present study

Compound	Starting materials	Reaction programme	Atmosphere
$Ca_4Nb_2O_9$	$CaCO_3 + Nb_2O_5$	1173 K for 12 h, 1648 K for 12 h × 2	Air
Li_5FeO_4	$Li_2O + Fe_2O_3$	973 K for 12 h	Argon
Li_6CoO_4	$Li_2O + CoO$	973 K for 12 h	Argon
Li_4SiO_4	$LiCO_3 + SiO_2$	1173 K for 12 h	Air
Li_5AlO_4	$Li_2O + Al_2O_3$	973 K for 12 h	Air
Mg_6MnO_8	$MgO + MnO_2$	1173 K for 12 h	Air
Na_3SbO_4	$Na_2CO_3 + Sb_2O_3$	923 K for 12 h, 1173 K for 12 h, 1223 K for 12 h	Air

The stoichiometric mixtures were ground using an agate mortar and pestle, except for the Mg_6MnO_8 starting materials, which were mixed thoroughly with a high energy ball mill (SPEX SamplePrep 8000M) for 1 hour. Phase purity of the samples was monitored by room-temperature X-ray powder diffraction (XRD), using a Panalytical Empyrean diffractometer utilising Cu K_α radiation. The Li_5FeO_4 and Li_6CoO_4 samples were seen to visibly react over the course of a day in air, as denoted by a distinct change in colour, owing to reaction with CO_2 in the air. XRD and TGA measurements confirmed the presence of Li_2CO_3 in these samples as a result of their reaction.

Thermogravimetry

The carbonation and calcination reactions of the candidate materials were investigated using a thermogravimetric analyser (TGA/DSC 1, Mettler Toledo) operating at atmospheric pressure. In each experiment, a sample of ~20 mg of powder was placed in a 70 μL Al_2O_3 or Pt crucible, supported on a cantilever-type balance. Gases were fed to the reaction chamber through three gas ports, viz. reactive gas, purge gas and protective gas. The reaction chamber was electrically heated by a tubular furnace surrounding the balance. Both the protective gas and

the purge gas were N_2, and were fed to the TGA reaction chamber with a flow rate of 50 mL min^{-1}. The reactive gas was a stream of pre-mixed N_2 and CO_2, fed by a capillary so that the gas could flow over the top of the crucible. The partial pressure of CO_2 at the surface of the solid sample was adjusted by varying the mix of N_2 and CO_2 in the reactive gas, while keeping a constant overall flow rate of 50 mL min^{-1}.

For the experiments on differential scanning calorimetry (DSC), the samples were first heated to 873 K under a flow of N_2, before being exposed to a pure stream of CO_2 for 10 minutes at a constant temperature. Integration of the heat flow curves over this time interval with a baseline set to the heat flow prior to carbonation gave the heat accumulated in the sample during carbonation.

The actual CO_2 concentration at the gas–solid interface was calibrated against the well-understood thermodynamic $CaO/CaCO_3$ carbonation equilibrium. For example, when a carbonated sample of pure CaO (98 wt%) was slowly heated in a specific mixture of CO_2 and N_2, the temperature at the onset of $CaCO_3$ decomposition was recorded and the corresponding CO_2 partial pressure in contact with the solid phase was determined from the phase diagram of the $CaO–CaCO_3–CO_2$ system. In the temperature-programmed decomposition (TPD) experiments, the samples were heated from 323 K to either 973 K (Li_6CoO_4 and Li_5FeO_4) or 1223 K ($Ca_4Nb_2O_9$, Mg_6MnO_8 and Na_3SbO_4) under a specific partial pressure of CO_2, i.e. a specific N_2/CO_2 ratio. The equilibrium temperature corresponding to a given partial pressure of CO_2 was determined by the temperature at which the material started to decompose (after possibly carbonating at a lower temperature), determined by the zero of the first derivative of the mass curve.

Surface measurements

The surface morphologies of the solid samples at various stages of the cycling experiments (viz. fresh, fully carbonated and fully regenerated) were examined ex situ by scanning electron microscopy (SEM). The samples were inspected in a field-emission gun SEM (Hitachi S-5500) with a secondary electron detector.

The porosity and specific surface area (SSA) of the candidate materials were determined using volumetric sorption measurements (TriStar3000 analyzer, Micromeritics) in N_2 at 77 K. The SSA was calculated using Brunauer–Emmett–Teller (BET) analysis using N_2 sorption.[39] Pore size distribution and pore volumes were determined by applying the Barrett–Joyner–Halenda (BJH) model using a 55 point adsorption–desorption isotherm.

Results and discussion

Summary of screened materials

The screening of the Materials Project database for compounds within the A–M–O–CO_2 open phase diagrams found 640 distinct compounds able to undergo reactions with CO_2, with a total of 1442 distinct carbonation reactions. The difference in these numbers is due to some compounds being able to undergo

Table 3 Total number of compounds and associated carbonation reactions found in the original screening, and after screening out compounds that either react with CO_2 below 293 K, or oxidise before carbonation

Alkali metal	Original screening		After filtering	
	Compounds	Reactions	Compounds	Reactions
Ba	91	195	60	121
Ca	74	164	32	46
K	101	261	73	191
Li	57	118	50	103
Mg	48	84	19	32
Na	92	249	71	187
Rb	81	175	60	135
Sr	75	165	59	122
Non-alkali	21	31	8	9
Total	640	1442	432	946

several different decomposition pathways with increasing CO_2 chemical potential. A breakdown of these numbers into separate alkali metal compounds can be seen in Table 3.

Two subsequent filters were applied to the results to screen realistically for materials that could be practically used for high temperature CO_2 absorption looping applications. The first filter removed materials whose decomposition reactions occurred below 293 K, as practically a CCS process would have to occur at room temperature or above. The second filter used a similar open phase diagram construction as used previously in the original screening process, except this time with the open element being O_2, to screen the materials for their stability at the very low p_{O_2} levels expected in the calciner, the reaction chamber where the carbonated materials are decomposed to release gaseous CO_2 and reform the original material ($p_{O_2} < 0.01$). Those materials that would reduce or even oxidise under these conditions were removed from the screening, as they would transform before the carbonation reaction had a chance to occur. The remaining distinct compounds, along with the number of distinct possible carbonation reactions, can be seen in Table 3.

These results show that the methodology was able to find materials that undergo carbonation reactions across all the different alkali metals used, and is certainly the largest number of solid oxide type materials ever to be considered for CCS applications in a single study. Interestingly, while a reasonable number of compounds are found in the database for the most abundant alkaline earth metals, Ca and Mg, these compounds are disproportionally removed by the filtering process. Potentially the stability of the binary oxides CaO and MgO compared to the other alkali binary oxides could simply result in fewer stable tertiary phases with these elements.

Calculated properties of screened materials

Using the relative energies of the reactant and product phases in each theoretical carbonation reaction it was possible to compute a value for $\Delta H_{carbonation}$.[30] For a single compound, the multiple reactions essentially describe the same decomposition process, followed to different endpoints, with the order following increasing $\Delta H_{carbonation}$. Experimentally, we only observed the products of the first decomposition reaction, even on increasing T, and therefore the results could be further

restricted to one carbonation reaction for each distinct compound, the reaction with the most negative $\Delta H_{carbonation}$.

In evaluating the theoretical energy penalties of the screened materials, the most commonly used high temperature CCS material, CaO, was used as a benchmark for comparison (with a calculated energy penalty of 41.9 kJ (mol CO_2)$^{-1}$). For reference, process engineering studies using CaO as a solid absorbent in a postcombustion CCS setup found this process imposes a 6–8% energy penalty as compared to plants without CCS,[40–42] and of that penalty, between 3–10% is attributed to the energy to calcine $CaCO_3$ to CaO. A commonly accepted goal for an economically-viable CCS process set by the US Department of Energy is to have an energy penalty of 5% or less, so if we assume that our calculated energy penalty mostly accounts for the calcination energy, this would mean finding a material in our screening with $E_p < 35$ kJ (mol CO_2)$^{-1}$. This is still only a rough approximation, as any promising candidate would also need to be subjected to in-depth process investigation to determine its realistic energy penalty in a CCS process.

From the stoichiometry of the reaction, it is also possible to determine the CO_2 gravimetric capacity ($g_{CO_2absorbed}/g_{sorbent}$) of

each theoretical carbonation reaction, as well as the volume change for the reaction (derived from the change in the unit cell volume of the optimised structures). There is some evidence to suggest that changes in volume contribute to the cycling instability of CaO, with large volume changes possibly causing pore closure and particle sintering and resulting in the rapid fading of the CO_2 capture efficiency over the first 10–20 cycles.[10,43–45] Therefore, the compounds were screened based on the volume change with carbonation as a preliminary indication of the stability of the compound over multiple cycles.

These different parameters were plotted for each of the screened reactions in Fig. 4. There is a direct correlation with ΔH and E_p, as expected considering it is a dominant part of the Q_{loss} and $Q_{recovered}$ terms used to determine the overall energy penalty (for more details see the ESI†). However, for less exothermic carbonation reactions, the magnitude of these terms is similar to that of the specific heat capacity term. The approximate specific heat capacities of the compounds used in the screening were calculated using the Dulong–Petit law,[46] this being a good approximation for solid state materials at high temperature, and also being trivial to calculate as it only
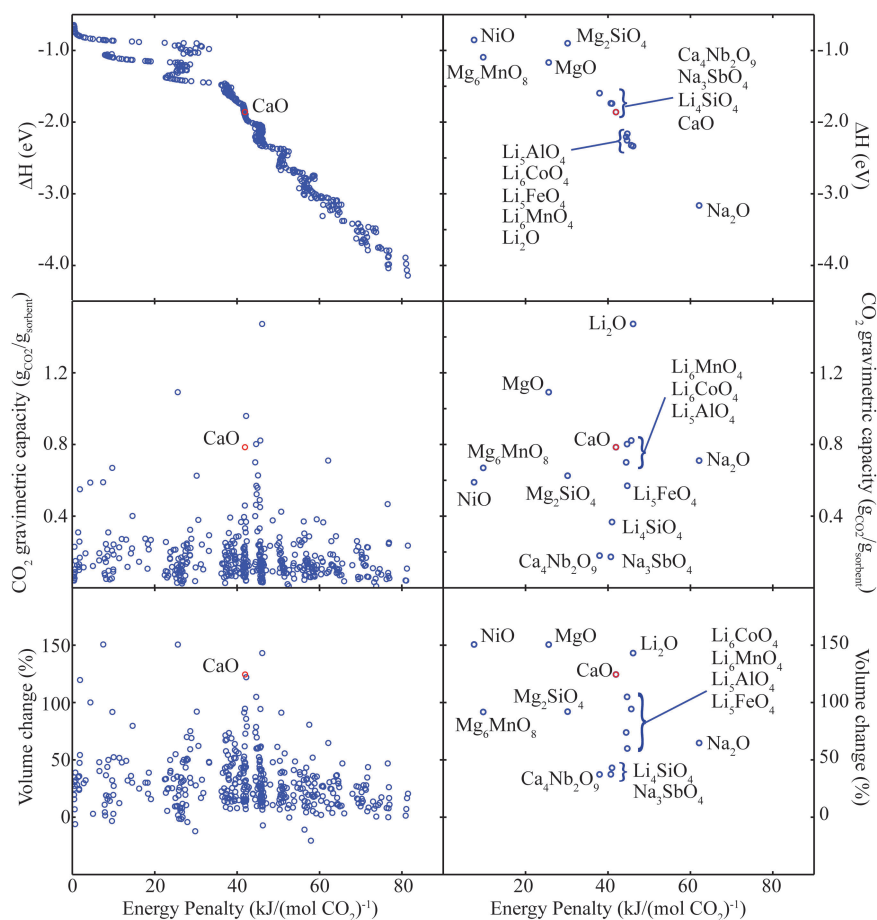

Fig. 4 Overview of results from the screening of the Materials Project database for compounds that undergo carbonation. Each data point represents the carbonation reaction for each distinct compound with the most negative ΔH. The calculated energy penalty, E_p, for each reaction is plotted against $\Delta H_{carbonation}$ (top), CO_2 gravimetric capacity (middle) and volume change (bottom). The plots on the left are for the complete 640 distinct compounds in the screening, and the plots on the right are for specific compounds of interest (including the five candidate materials).

1352 | *Energy Environ. Sci.*, 2016, **9**, 1346–1360

This journal is © The Royal Society of Chemistry 2016

depends on the molar mass (MM) of the compound. In the lower energy penalty part of the plot, some materials are seen with similar E_p, but with ΔH that differ by as much as 0.5 eV. In this region some control is possible over the balance between ΔH and MM to achieve a given E_p, and given that compounds with a lower MM will normally have a higher gravimetric CO_2 capacity, this means it is possible to select compounds on the basis of this parameter. Conversely, for a process requiring a smaller ΔH to reduce heat flow in and out of the system, it is possible to select compounds with a higher MM to achieve the same overall E_p.

Selection of candidate materials

Our experimental studies focussed on five materials with previously unreported CCS properties: Mg_6MnO_8, $Ca_4Nb_2O_9$, Na_3SbO_4, Li_5FeO_4 and Li_6CoO_4. Mg_6MnO_8 has a much lower theoretical E_p than CaO and a comparably high gravimetric CO_2 capacity, making it a promising material for future applications. $Ca_4Nb_2O_9$ and Na_3SbO_4 were chosen because they had similar, but lower E_p values than that of CaO from the screening, and as such they represent useful comparisons to the benchmark material, especially in comparing their cycling stability and the effect of adding a third element to the binary Ca–O phase diagram (in the case of $Ca_4Nb_2O_9$). Li_5FeO_4 and Li_6CoO_4 were chosen for their very high theoretical gravimetric CO_2 capacities, and for comparison to previous studies on similar Li ternary oxides.[47–51] It should be noted, however, that Na_3SbO_4 and Li_6CoO_4 are unlikely to find use in CCS applications owing to the cost of Sb and the toxicity of Co, although $Ca_4Nb_2O_9$, Mg_6MnO_8 and Li_5FeO_4 are made from more abundant and safe elements and are thus particularly appealing. The relevant parameters obtained from the Materials Project screening for these materials are presented in Table 4.

Initial post-carbonation structural characterisation

XRD patterns acquired of the as-synthesised Mg_6MnO_8, $Ca_4Nb_2O_9$, Na_3SbO_4, Li_5FeO_4 and Li_6CoO_4 samples confirmed that all these materials were mostly a single pure phase, with some small impurity phases present in the case of Na_3SbO_4. BET surface area analysis was also performed on the materials, showing them to have similarly low surface areas, consistent with oxides sintered at high temperatures (results available in the ESI†). Further XRD

patterns were then taken of these samples after being carbonated under $p_{CO_2} = 0.37$ bar at 773 K (Mg_6MnO_8), 973 K (Li_5FeO_4 and Li_6CoO_4) or 1223 K (Na_3SbO_4 and $Ca_4Nb_2O_9$) in a thermogravimetric analyser (TGA) to identify the phases that formed upon carbonation, and to see if these match with the phases predicted by the screening. Carbonation temperatures were identified by an initial TGA experiment to determine the range over which the samples carbonated and regenerated. For Na_3SbO_4, Li_5FeO_4 and Li_6CoO_4, phases present in the pre- and post-carbonation samples could be indexed and their structures and cell parameters were refined using Rietveld refinement, as shown in Fig. 5. For Li_5FeO_4 a significant amount of the original material remained after carbonation (19% by weight), indicating that the reaction had not gone to completion.

Unfortunately in the case of Mg_6MnO_8 and $Ca_4Nb_2O_9$, even after multiple attempts to carbonate the samples at different temperatures and over longer time periods, no evidence for reaction could be found in their XRD diffractograms. Subsequent TGA experiments showed that the materials increased their weight by a very small amount close to the detection limit of the instrument (~ 0.01 mg) when heated under flowing CO_2, which likely is undetectable by diffraction. As these samples were essentially unreactive with CO_2 they were excluded from any further analysis.

Carbonation experiments

In order to determine $\Delta H_{carbonation}$ and $\Delta S_{carbonation}$, the equilibrium constants of the respective carbonation reactions as a function of temperature were measured experimentally by TPD in a TGA under various CO_2 partial pressures, with a typical trace for Na_3SbO_4 shown in Fig. 6. As described in previous studies,[29] the equilibrium curve for a carbonation reaction can be fitted by an exponential curve of the form:

$$K_p = p_{CO_2} = A \exp\left(-\frac{B}{T}\right) \quad (5)$$

where p_{CO_2} is the CO_2 partial pressure in atm, T is calcination temperature in K, and A and B are constants specific to each reaction, which can be obtained by plotting a logarithmic curve of $1/T$ measured at different p_{CO_2}.

From these it is possible to calculate $\Delta H_{carbonation}$ and $\Delta S_{carbonation}$ from these fitting constants, assuming that $\Delta H_{carbonation}$ and $\Delta S_{carbonation}$ are approximately constant:

$$K_p = \exp(\Delta S_r/R)\cdot\exp(-\Delta H_r/RT) \quad (6)$$

$$A = \exp(\Delta S_r/R) \quad (7)$$

$$B = \Delta H_r/R \quad (8)$$

The fits for the constants A and B for Na_3SbO_4 and Li_4SiO_4 (as an example of a promising material studied previously for CCS[49]) are shown in Fig. 7, and then compared against the corresponding values obtained from the Materials Project screening in Table 5. Attempts to perform a similar TPD analysis for Li_5FeO_4 and Li_6CoO_4 failed because the phases formed in the carbonation reactions do not decompose before the melting point of Li_2CO_3 at ~ 993 K, even though the

Table 4 Theoretical screening results for CaO and the preliminary candidates in the experimental analysis. The respective carbonation reactions relating to the tabulated values are CaO + CO_2 → $CaCO_3$; $Ca_4Nb_2O_9$ + $2CO_2$ → $2CaCO_3$ + $Ca_2Nb_2O_7$; Mg_6MnO_8 + $5CO_2$ → $5MgCO_3$ + $MgMnO_3$; Na_3SbO_4 + CO_2 → Na_2CO_3 + $NaSbO_3$; $0.5Li_5FeO_4$ + CO_2 → Li_2CO_3 + $0.5LiFeO_2$; and $0.33Li_6CoO_4$ + CO_2 → Li_2CO_3 + $0.33CoO$

Compound	E_p (kJ (mol CO_2)$^{-1}$)	$\Delta H_{carbonation}$ (kJ mol^{-1})	CO_2 capacity ($g_{CO_2}/g_{sorbent}$)	Volume change (%)
CaO	41.9	−179.5	0.78	124.4
Mg_6MnO_8	9.7	−105.6	0.67	91.7
$Ca_4Nb_2O_9$	37.9	−153.9	0.18	37.3
Na_3SbO_4	40.7	−167.6	0.17	37.4
Li_5FeO_4	44.7	−208.7	0.57	59.9
Li_6CoO_4	44.6	−217.4	0.80	104.9

This journal is © The Royal Society of Chemistry 2016
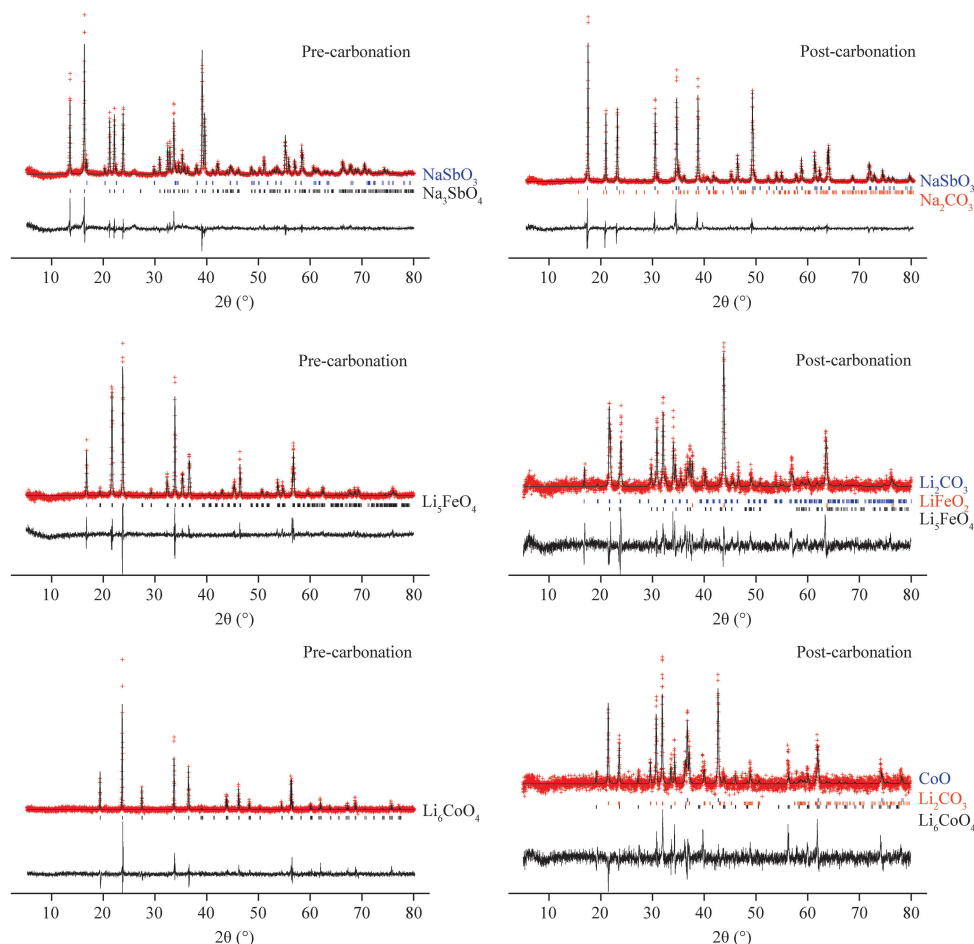
Energy Environ. Sci., 2016, **9**, 1346–1360 | **1353**

Fig. 5 Indexed XRD diffractograms (λ = 1.54056 Å) and refinements of the as-synthesised Na_3SbO_4, Li_5FeO_4 and Li_6CoO_4 samples, and after carbonation at 973 K (Li_5FeO_4 and Li_6CoO_4) or 1223 K (Na_3SbO_4) under p_{CO_2} = 0.37 bar. The experimental data points are shown in red, with the pattern obtained from the Rietveld refinements overlaid in black, and the difference curve below.
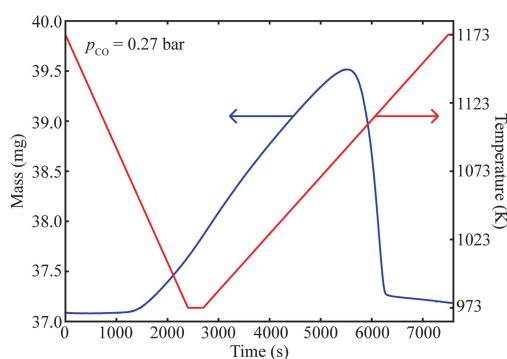

Fig. 6 Temperature programmed decomposition (TPD) experiment for Na_3SbO_4 at p_{CO_2} = 0.27 bar. The mass gain corresponds to the carbonation reaction $Na_3SbO_4 + CO_2 \rightarrow Na_2CO_3 + NaSbO_3$. Calculation of the zero point of the first derivative of the mass curve gives the temperature of the onset of decomposition.

temperature of decomposition was predicted to be $\sim$805 K at p_{CO_2} = 1 from the screening. TPD traces of Li_5FeO_4 and Li_6CoO_4 are given in Fig. 8, showing the mass gains as the materials react with CO_2 to form Li_2CO_3 and $LiFeO_2$ or CoO respectively. Upon further heating, however, there is no mass loss, and

therefore the same method of determining the carbonation equilibrium constant cannot be used. It is also seen in these TGA traces that the experimental CO_2 capacity is much less than the theoretical value as obtained from the stoichiometry of the carbonation reaction. One reason for this may be that a large percentage of the sample had already reacted with CO_2 in the air prior to the experiment, as it was not possible to keep the samples in vacuum when transferring in and out of the TGA itself. Furthermore, longer isothermal experiments should be performed in future studies to better elucidate the combined effect of thermodynamics and kinetics on the rate of these reactions.

For the materials studied, it is seen that there is very good agreement between the theoretical and experimental values for $\Delta H_{carbonation}$. In the case of CaO, this is to be expected because of the CO_2 energy correction applied which was derived from experimental values for binary oxide carbonation reactions. But for Na_3SbO_4 and Li_4SiO_4, these results validate the accuracy of the screening process and its ability to predict correctly the carbonation equilibrium for both current promising CCS materials and also for previously unstudied materials. Fairly large errors are often seen in TPD fitting, especially because of the sensitivity between any small amount of scatter in the TGA
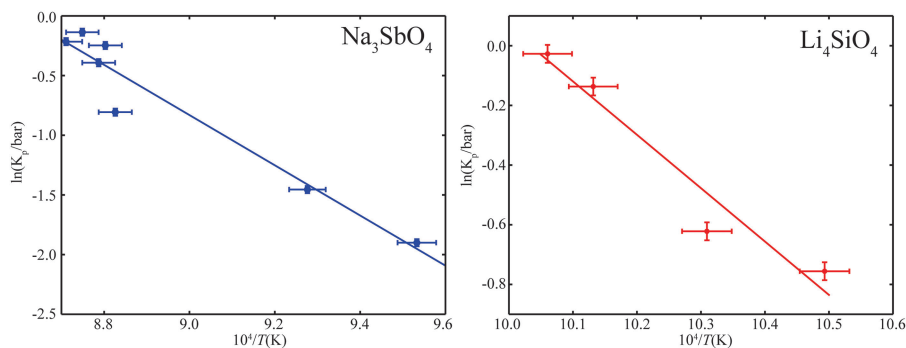
1354 | *Energy Environ. Sci.*, 2016, **9**, 1346–1360

This journal is © The Royal Society of Chemistry 2016

Fig. 7 Plot of $\ln(K_p)$ against the inverse decomposition onset temperatures derived from TPD experiments for Na_3SbO_4 and Li_4SiO_4. The linear fit to determine the constants A and B relating to K_p is also shown on each plot.

Table 5 Experimentally derived values and predicted values from the Materials Project screening of $\Delta H_{carbonation}$ and $\Delta S_{carbonation}$ for CaO, Na_3SbO_4 and Li_4SiO_4. The screening values are based on the following reactions: $CaO + CO_2 \rightarrow CaCO_3$, $Na_3SbO_4 + CO_2 \rightarrow Na_2CO_3 + NaSbO_3$ and $Li_4SiO_4 + CO_2 \rightarrow Li_2CO_3 + Li_2SiO_3$

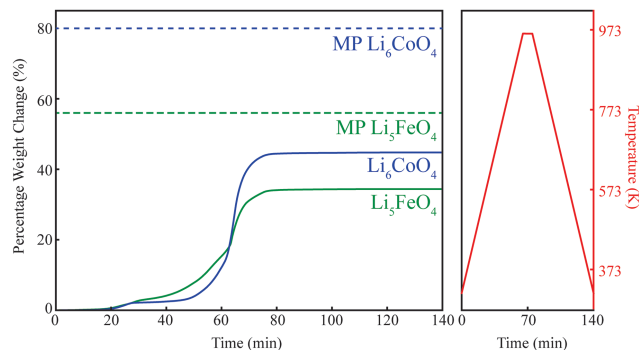| | Experimental | | Screening |
Compound	ΔH_r (kJ mol^{-1})	ΔS_r (J mol^{-1} K^{-1})	ΔH_r (kJ mol^{-1})
CaO	-170 ± 5	152 ± 5	-179.5
Na_3SbO_4	-175 ± 26	150 ± 23	-167.6
Li_4SiO_4	-149 ± 58	149 ± 59	-167.9

Fig. 8 TGA traces for Li_5FeO_4 and Li_6CoO_4 under $p_{CO_2} \approx 0.1$ bar.

data (which can be due to instrumental factors) and the enthalpy and entropy values that are eventually derived.

Determination of carbonation enthalpy by DSC

For materials whose carbonation products melt before decomposing, such as Li_5FeO_4 and Li_6CoO_4, DSC experiments provide an alternative way to determine $\Delta H_{carbonation}$ without melting the material. Integrated heat curves for the candidate materials, CaO and Li_5AlO_4 (as an example of a another similar material studied previously for CCS[51,52]) derived from DSC are shown in Fig. 9. By taking a TGA trace simultaneously, the mass change of the sample can be measured over the same time interval, and calculating the CO_2 absorbed in moles allows $\Delta H_{carbonation}$ in kJ mol^{-1} to be derived:

$$\Delta H = \int_1^2 \frac{dH}{dt} dt \tag{9}$$

The results are shown in Table 6 for experiments performed isothermally at 873 K.

Comparing the $\Delta H_{carbonation}$ for CaO obtained from DSC, -157 kJ mol^{-1}, with the known experimental value of -169 kJ mol^{-1},[53] it is seen that while the DSC method tends to underestimate $\Delta H_{carbonation}$ by $\sim 10\%$, it can still be used as an approximate experimental guide. For Li_5FeO_4 and Li_5AlO_4 there
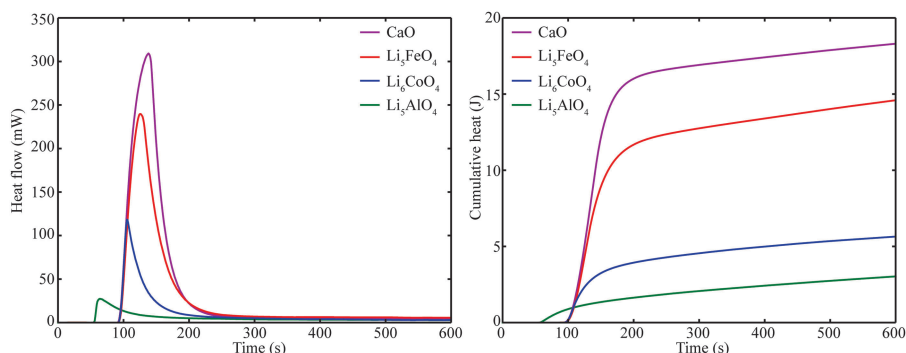

Fig. 9 DSC obtained heat flow and cumulative heat traces for CaO, Li_5FeO_4, Li_6CoO_4 and Li_5AlO_4 samples, studied isothermally at 823 K under $p(CO_2) = 1$ bar. There is a lag of $\sim 60-100$ s before carbonation begins due to the change of reactive gas flow in the TGA between pure N_2 and pure CO_2. The difference in lag between the trace for Li_5AlO_4 and the other samples is due to the use of a slightly different gas flow setup which uses valves to change between gases more quickly.

Table 6 Values of $\Delta H_{carbonation}$ obtained from DSC and TPD experiments compared with literature and the predicted values from the Materials Project screening. All values are in kJ mol^{-1}

Compound	DSC ΔH_r	TPD ΔH_r	Screening ΔH_r	Literature ΔH_r
CaO	-157 ± 5	-170 ± 5	-179.5	-169 ± 4[53]
Li$_5$FeO$_4$	-197 ± 5		-208.7	
Li$_6$CoO$_4$	-158 ± 5		-217.4	
Li$_5$AlO$_4$	-195 ± 5		-212.8	

is a reasonably good agreement between the experimental and theoretical values, within error. For Li$_6$CoO$_4$ the theoretical value is $\sim 30\%$ higher than that obtained from the DSC experiment. Further thermogravimetric tests to gain a more accurate experimental value of $\Delta H_{carbonation}$ are ongoing, specifically TPD experiments under more precisely determined $p(CO_2)$ and ramp rates, which will allow greater confidence when comparing to the values obtained from the Materials Project.

CO$_2$ cycling capacity studies

To further investigate the cycling performance of the novel CCS material Na$_3$SbO$_4$, the sample was heated between 923 K and 1173 K for 40 minutes each to sequentially carbonate and decarbonate the material. The switches between temperatures were achieved by heating and cooling at constant rates of 20 K min^{-1} and -20 K min^{-1}, respectively, all under a constant CO$_2$ partial pressure of 0.1 bar in contact with the solid sample. The results of the cycling experiments were analysed by estimating the CO$_2$ uptake ($g_{CO_2}/g_{sorbent}$) by the sorbent in each cycle according to:

$$CO_2\,uptake = \frac{m_{max,i} - m_{min,i}}{m_{min,i}} \quad (10)$$

where $m_{max,i}$ and $m_{min,i}$ are the maximum and minimum mass of the sample in the ith cycle respectively. The profile of CO$_2$ uptake, as a function of cycle number, is plotted in Fig. 10a.

The results show that Na$_3$SbO$_4$ carbonates at close to full theoretical capacity on the first cycle, but shows capacity fading upon further cycling. In particular, the capacity of Na$_3$SbO$_4$ rapidly decreases even by the second cycle, which showed

approximately half the CO$_2$ uptake compared to the first cycle. It settles to a gravimetric capacity of $\sim 0.035\ g_{CO_2}/g_{sorbent}$ after 24 cycles, which is roughly half the gravimetric capacity displayed by CaO under similar conditions.[10]

Further analysis of the maximum and minimum sample masses measured during each cycle reveals that the reduction in capacity is almost entirely due to the decreasing maximum sample mass measured in each cycle, compared to the minimum sample mass which stays relatively constant (Fig. 10b). The minimum mass corresponds to the mass of the fully regenerated sample, and as such these results indicate that the sample is regenerating fully upon each cycle. The reduction in the maximum sample mass shows that the capacity fading is primarily due to the reduced amount of carbonate being formed in each cycle.

These results indicate that volume change might not be sufficient to indicate materials which might have improved cycling stability, and that capacity fading is a more complex process than can be described by a single variable.

Morphological studies of materials upon cycling

To further investigate the reasons for the degradation of CO$_2$ capacity experienced by Na$_3$SbO$_4$ upon cycling, the sample was observed using SEM across a number of carbonation cycles, as shown in Fig. 11.

The SEM results indicate that, like CaO and MgO, the capacity of Na$_3$SbO$_4$ to absorb CO$_2$ is limited by the extent of carbonation, which is a strong function of the surface morphology.[10,54] The fresh particles (images (a) and (b)) show a large amount of available surface area, allowing the maximum amount of reaction with gaseous CO$_2$. It is much more difficult to distinguish two different phases in the carbonated samples (images (c) and (d)); instead, there appears to be a phase formed with a different morphology and reduced surface area and porosity. This is presumably Na$_2$CO$_3$, which sinters because the sample was close to its melting point. The images of the fully regenerated particle after 20 cycles (images (e) and (f)) show that the morphology mirrors that of the carbonated phase, indicating that this sintering persists even upon regenerating the
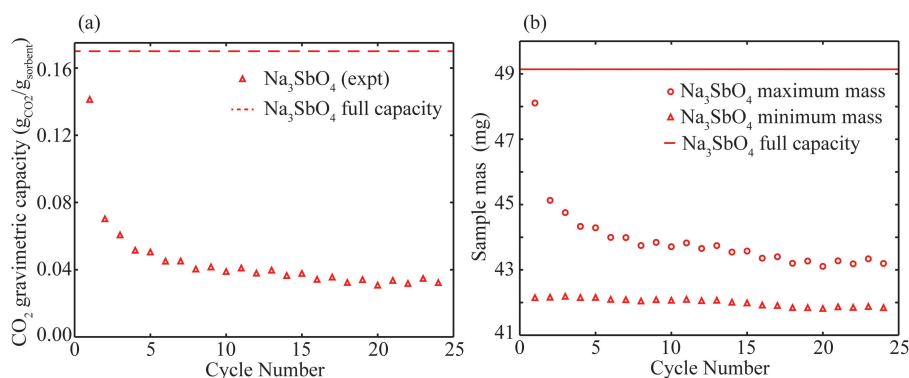

Fig. 10 (a) Gravimetric CO$_2$ capacity as a function of cycle number for Na$_3$SbO$_4$, measured by TGA under $p(CO_2)$ = 0.1 bar. The full and dashed lines show the predicted capacity, based on the stoichiometry of the carbonation reaction. Na$_3$SbO$_4$ initially absorbs CO$_2$ at close to full theoretical capacity, but its capacity quickly fades to between 25–35% of that of the first cycle. (b) Maximum and minimum sample masses measured during each cycle for Na$_3$SbO$_4$.
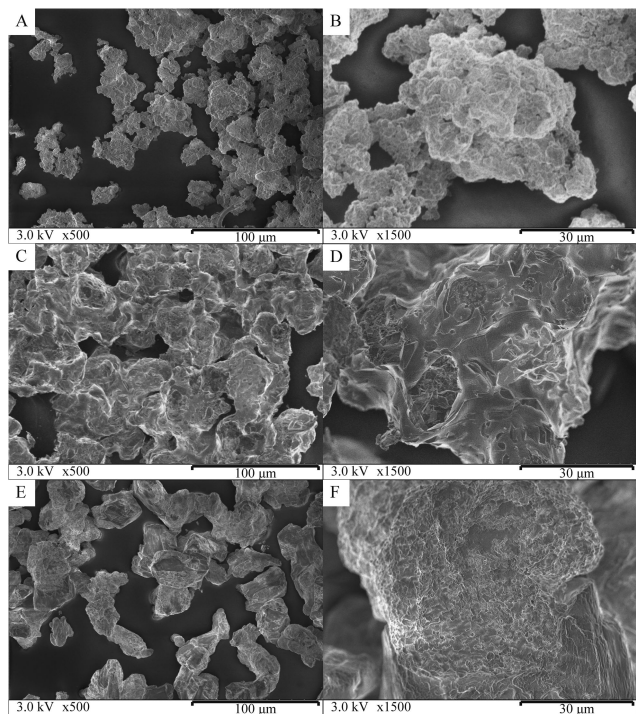
Fig. 11 SEM images of Na_3SbO_4 samples under two different magnifications (left: ×500, right: ×1500): heated to 1223 K under N_2 (A) and (B); fully carbonated (C) and (D); and cycled 20 times, then fully regenerated under N_2 (E) and (F). Upon extended cycling Na_3SbO_4 shows a drastic decrease in both surface area and available porosity, which is likely responsible for its reduction in cycling capacity. The drastic reduction in surface area can be seen especially in the cycled material (F) as compared to the unreacted material (B), indicating that this is a key parameter influencing the cycling stability of Na_3SbO_4.

sample, and that multiple cycles appear to lock in this reduction of surface area and porosity. This would seem to explain the reduction in carbonation capacity of these cycled particles as there is less available surface area for CO_2 to react with. These results indicate that thermodynamic parameters influencing the ability to fully regenerate the original material, as well as finding ways to control the surface morphology of the sorbents over many cycles, are key to finding a material with a stable cycling capacity. Both parameters influence the overall behaviour of a sorbent, and only focussing on a single aspect is insufficient to define a material's ability to withstand multiple carbonation cycles without losing capacity.

Discussion

Regarding gravimetric CO_2 capacity, CaO has one of the highest capacities amongst the compounds screened, due to it having a very small molecular mass (MM) that is able to react with 1 mol of CO_2 (and which makes it particularly desirable for use in CCS). Similarly, the other binary oxides screened also had very high gravimetric capacities due to their small MM. The addition of ternary elements that do not directly take part in the carbonation reaction and simply lead to the formation of

secondary reaction products would be thought to result in such ternary materials generally having very low capacities. However, there are some ternary compounds that show comparable capacities, such as the compounds with very high alkali metal content Li_5FeO_4, Li_6CoO_4 and Mg_6MnO_8. While it is important to have a high theoretical CO_2 capacity, in practice a low E_p is more desirable in terms of reducing costs, so a lower capacity can be offset with a lower E_p to still produce a material that is promising for CCS applications.

If we take volume change to be one indicator of a compound's resistance to capacity fading upon cycling, the spread of results confirms that there is a wide composition space in which to find more optimal materials with improved properties compared to CaO. In particular, CaO had one of the highest volume increases upon carbonation (124%) out of all the materials screened, with only the binary compounds NiO, MgO and Li_2O having a larger volume expansion. However, a large volume change is not always determinental, as seen in materials such as $Ba_4Sb_2O_9$ which displays a large change in volume upon reaction, but also did not fade in capacity over 100 cycles.[29]

Fig. 12 further filters the screened compounds to include only those where A = Na, Li, Mg or Ca, to make a more direct comparison of our screening results with the kinds of materials that have been suggested previously in the literature, composed of these metals. It is clear from Fig. 12 that the carbonation equilibrium is greatly influenced by the choice of metal atom, with Na-based compounds having the most negative $\Delta H_{carbonation}$ and hence the largest E_p, while Ca and Mg based compounds have a much lower E_p generally. In particular, there seem to be many Mg-based materials with relatively low E_p that could have a desirable carbonation equilibrium. For example, the screening found two ternary Mg-based compounds with very high gravimetric capacity: Mg_2SiO_4 or olivine, which has already been researched extensively as a geological CCS material[55] and Mg_6MnO_8, which unfortunately when investigated in the present study was found to be extremely unreactive. The poor reactivity of Mg_6MnO_8 could be due to either poor intrinsic kinetics or mass transport in the material. Similar to MgO, these materials carbonate at much lower temperatures than Ca-based materials, explaining the much slower reaction kinetics (which are compounded by a generally smaller enthalpic driving force for the carbonation reaction). Further studies are intended to optimise this material's reactivity potentially through producing a sample with smaller particles that might improve its carbonation kinetics, although grinding a material to increase its reactivity introduces a further energy cost to the overall process.

The range of $\Delta H_{carbonation}$ and E_p within members of the same alkali or alkaline-earth metal group seems directly related to the relative stability of the corresponding binary alkali metal oxides, which are the reactive species in all of the carbonation reactions (regardless of what other metal atoms might be present), and in the majority of cases the addition of a ternary element increases $\Delta H_{carbonation}$ and decreases E_p. This would suggest that there is a good thermodynamic reason for pursuing ternary alkali compounds as novel CCS materials and moving beyond using simple binary oxides.
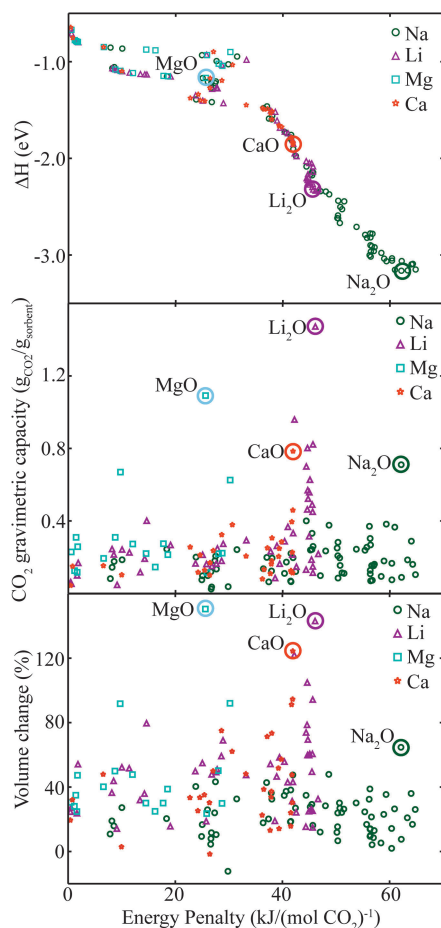
This journal is © The Royal Society of Chemistry 2016

Energy Environ. Sci., 2016, **9**, 1346–1360 | **1357**

Fig. 12 Screened materials containing Na, Li, Mg or Ca as their alkali atom. Each data point represents the carbonation reaction for each distinct compound with the most negative ΔH. The calculated energy penalty, E_p, for each reaction is plotted against $\Delta H_{carbonation}$ (top), CO_2 gravimetric capacity (middle) and volume change (bottom). The respective binary oxides are circled for clarity.

In terms of gravimetric CO_2 capacity, obviously the screening results reflect the fact that the binary oxides have the highest capacities, which is why they are so attractive for further development. However, there are a suite of ternary compounds with significant capacity, especially amongst Li-based compounds. Some of these have already been explored, such as Li_2ZrO_3,[47] Li_5AlO_4[51] and Li_4SiO_4,[49] but this screening has found many others, such as Li_6CoO_4, Li_6MnO_4 and Li_5FeO_4, that could be the subject of further research.

Volume change is perhaps the least important parameter to optimise for, as it is still not fully understood how large a role it plays in determining the cycling stability of a material. However, given the influence volume change has on the morphology of cycled materials and their subsequent reactivity, it is still a worthwhile measurement to include in our methodology. Furthermore, our results show that the binary oxides have the largest volume change upon cycling, further underscoring the necessity to pursue development of ternary alkali oxides as materials of interest which might have more moderate volume changes. Melting points of the phases involved, especially the carbonate phases, may also be an important parameter to include in future screening studies. Having a lower melting point generally leads to the cycled materials having lower remaining available porosity due to the earlier onset of sintering at the Tamman temperature (generally defined to be half the melting point of the material) and hence a smaller cycling capacity.

A further insight that cannot be ignored is the role of kinetics in finding a suitable CCS sorbent. The apparent failure of Mg_6MnO_8 and $Ca_4Nb_2O_9$, despite their very promising predicted capabilities, shows that any relevant future large scale screening approach must consider a way to build in reaction kinetics into its rational design algorithm. In this particular case the discrepancies between theory and experiment manifest from different causes for Mg_6MnO_8 and $Ca_4Nb_2O_9$. In the case of Mg_6MnO_8, similar Mg-based minerals such as olivine and even the binary oxide MgO are known to have very poor carbonation kinetics in the solid state, requiring radically different approaches to improve their performance such as including H_2O in the gas stream.[56,57] For $Ca_4Nb_2O_9$, it is likely that the much higher sintering temperature (1648 K) leads to a loss in available surface area for reaction, and hence leads to the slower overall carbonation kinetics.

One idea is to adapt an approach used for framework materials that characterises the internal surface volume and connected porosity of materials from their structure to estimate the kinetic barriers to gas diffusivity in these materials.[58] Conversely, it also means that more in-depth work to optimise promising materials may be needed to overcome these kinetic issues, lest excellent materials be missed after initial properties testing.

An additional factor that may also influence the actual performance of the screened materials is that of H_2O in the reactant gas stream. All our experiments and screening were performed in dry conditions, but this is not the case in most flue gases, which typically contain $\sim 10\%$ H_2O. Previous studies on similar materials to those found in our screening, most notably Li_4SiO_4[59] and Li_5AlO_4,[60] found that the addition of H_2O to the CO_2 gas stream results in a drastic decrease in carbonation reaction temperature. Such a decrease would result in a lower calculated energy penalty when compared to the results from our screening in dry conditions. Therefore, many of the materials studied in this work may in fact show even better performances in more realistic reactor conditions, and future work is planned to include H_2O in both the theoretical and experimental approaches outlined here.

Finally, given our recent work on novel CCS material, $Ba_4Sb_2O_9$,[29] a material that was previously not characterised and therefore not in the Materials Project database, underlines the importance of continually working to expand the database with new compositions, either from theory or experiment. Predicting new compositions and structures based on ternary oxides containing the abundant alkali metals Na, Mg and Ca using the Structure Predictor module already present in the Materials Project system[61] is a direction considered for further study.

1358 | *Energy Environ. Sci.*, 2016, **9**, 1346–1360

This journal is © The Royal Society of Chemistry 2016

Conclusions

Through the use of open phase diagrams and the Materials Project, the largest set to date of oxide compounds were screened for their theoretical thermodynamics of carbonation, as well as their theoretical gravimetric CO_2 capacity and volume change upon carbonation. The results were validated both against standard experimental values for known carbonation reactions, and against similar previous DFT studies, and good agreement was found with both. A single parameter, energy penalty, was used to assess the relative efficiency of using a compound in a model CCS process, and to provide a way to rank materials in terms of their suitability for further study.

Using a variety of thermogravimetric techniques, experimental validation was provided for a small set of candidate materials suggested by the Materials Project screening. For some of the materials, such as Na_3SbO_4 and Li_5FeO_4, the experimental values of $\Delta H_{carbonation}$ were in good agreement with those calculated from the screening procedure, indicating that the output of that screening can predict the carbonation thermodynamics of materials from a theoretical standpoint. This experimental validation is vital to developing a robust screening procedure that is able to predict materials that function under realistic reaction conditions.

Furthermore, the screening results give new insights to implement in rational design approaches towards finding optimal CCS materials. Firstly, the use of ternary alkali metal oxide compounds is found to be advantageous both in being able to achieve lower energy penalties due to less negative $\Delta H_{carbonation}$, but also in avoiding very large volume changes that occur when carbonating the binary oxide compounds, which could lead to cycling instability through sintering and pore clogging.

The alkali earth metals Mg and Ca are found to be generally more favourable than compounds containing Li and Na mainly due to their lower energy penalty, and there are many compounds found in the screening that are suitable for further study. However, subsequent experimental results found that Mg-based materials in particular display poor reaction kinetics, and require further optimisation in order to be used. These results show that large scale screening processes can employ a reasonably efficient level of DFT theory to achieve accurate results that give real information into overall trends that are important to designing novel functional materials.

Cycling experiments on Na_3SbO_4 showed that this material suffers similar capacity fading as seen in the CaO–$CaCO_3$ system, despite it having much lower predicted volume expansion upon carbonation. SEM studies suggest that the decrease in available surface area of the cycled particles compared to those in the fresh sample contributes to this capacity fading, and that some amount of the carbonate phase does not regenerate in later cycles. Future studies on a wider range of compounds will hopefully assist in understanding the underlying parameters influencing the stability of these compounds over many cycles of carbonation.

These results show that large scale screening processes can employ a reasonably efficient level of DFT theory to achieve accurate results that give real information into overall trends that are important to designing novel functional materials. As more sophisticated high-throughput methods are devised it will be increasingly possible to target functional materials with an array of complex and useful properties all before entering the laboratory.

Acknowledgements

References

1 Intergovernmental Panel on Climate Change, *Climate Change 2013 – The Physical Science Basis*, Cambridge University Press, Cambridge, 2014.
2 S. Pacala, *Science*, 2004, **305**, 968–972.
3 G. Férey, *Chem. Soc. Rev.*, 2008, **37**, 191.
4 O. M. Yaghi, M. O'Keeffe, N. W. Ockwig, H. K. Chae, M. Eddaoudi and J. Kim, *Nature*, 2003, **423**, 705–714.
5 D. M. D'Alessandro, B. Smit and J. R. Long, *Angew. Chem., Int. Ed.*, 2010, **49**, 6058–6082.
6 R. Banerjee, A. Phan, B. Wang, C. Knobler, H. Furukawa, M. O'Keeffe and O. M. Yaghi, *Science*, 2008, **319**, 939–943.
7 A. D. Ebner and J. A. Ritter, *Sep. Sci. Technol.*, 2009, **44**, 1273–1421.
8 E. J. Anthony, *Ind. Eng. Chem. Res.*, 2008, **47**, 1747–1754.
9 M. E. Boot-Handford, *et al.*, *Energy Environ. Sci.*, 2014, **7**, 130.
10 J. C. Abanades and D. Alvarez, *Energy Fuels*, 2003, **17**, 308–315.
11 Z.-S. Li, N.-S. Cai and Y.-Y. Huang, *Ind. Eng. Chem. Res.*, 2006, **45**, 1911–1917.
12 J. S. Dennis and R. Pacciani, *Chem. Eng. Sci.*, 2009, **64**, 2147–2157.
13 A. M. Kierzkowska, R. Pacciani and C. R. Müller, *ChemSusChem*, 2013, **6**, 1130–1148.
14 L.-C. Lin, A. H. Berger, R. L. Martin, J. Kim, J. A. Swisher, K. Jariwala, C. H. Rycroft, A. S. Bhown, M. W. Deem, M. Haranczyk and B. Smit, *Nat. Mater.*, 2012, **11**, 633–641.
15 J. M. Huck, L.-C. Lin, A. H. Berger, M. N. Shahrak, R. L. Martin, A. S. Bhown, M. Haranczyk, K. Reuter and B. Smit, *Energy Environ. Sci.*, 2014, **7**, 4132–4146.
16 R. Krishna and J. M. van Baten, *Phys. Chem. Chem. Phys.*, 2011, **13**, 10593.

This journal is © The Royal Society of Chemistry 2016

Energy Environ. Sci., 2016, **9**, 1346–1360 | 1359

17 R. Krishna and J. R. Long, *J. Phys. Chem. C*, 2011, **115**, 12941–12950.

18 A. Ö. YazaydÄśn, R. Q. Snurr, T.-H. Park, K. Koh, J. Liu, M. D. LeVan, A. I. Benin, P. Jakubczak, M. Lanuza, D. B. Galloway, J. J. Low and R. R. Willis, *J. Am. Chem. Soc.*, 2009, **131**, 18198–18199.

19 Y. Duan, *J. Renewable Sustainable Energy*, 2011, **3**, 013102.

20 Y. Duan, B. Zhang, D. C. Sorescu and J. K. Johnson, *J. Solid State Chem.*, 2011, **184**, 304–311.

21 Y. Duan, *Phys. Chem. Chem. Phys.*, 2013, **15**, 9752.

22 Y. Duan and D. C. Sorescu, *J. Chem. Phys.*, 2010, **133**, 074508.

23 Y. Duan, *Int. J. Clean Coal Energy*, 2012, **1**, 1–11.

24 A. Jain, S. P. Ong, G. Hautier, W. Chen, W. D. Richards, S. Dacek, S. Cholia, D. Gunter, D. Skinner, G. Ceder and K. A. Persson, *APL Mater.*, 2013, **1**, 011002.

25 G. Kresse, *Phys. Rev. B: Condens. Matter Mater. Phys.*, 1996, **54**, 11169–11186.

26 G. Kresse and J. Furthmüller, *Comput. Mater. Sci.*, 1996, **6**, 15–50.

27 S. P. Ong, S. Cholia, A. Jain, M. Brafman, D. Gunter, G. Ceder and K. A. Persson, *Comput. Mater. Sci.*, 2015, **97**, 209–215.

28 S. P. Ong, W. D. Richards, A. Jain, G. Hautier, M. Kocher, S. Cholia, D. Gunter, V. L. Chevrier, K. A. Persson and G. Ceder, *Comput. Mater. Sci.*, 2013, **68**, 314–319.

29 M. T. Dunstan, W. Liu, A. F. Pavan, J. A. Kimpton, C. D. Ling, S. A. Scott, J. S. Dennis and C. P. Grey, *Chem. Mater.*, 2013, **25**, 4881–4891.

30 A. Jain, G. Hautier, S. P. Ong, C. J. Moore, C. C. Fischer, K. A. Persson and G. Ceder, *Phys. Rev. B: Condens. Matter Mater. Phys.*, 2011, **84**, 045115.

31 S. P. Ong, L. Wang, B. Kang and G. Ceder, *Chem. Mater.*, 2008, **20**, 1798–1807.

32 S. P. Ong, A. Jain, G. Hautier, B. Kang and G. Ceder, *Electrochem. Commun.*, 2010, **12**, 427–430.

33 J. H. Wang and M. Liu, *J. Power Sources*, 2008, **176**, 23.

34 J. J. Xie, S. de Gironcoli, S. Baroni and M. Scheffler, *Phys. Rev. B: Condens. Matter Mater. Phys.*, 1999, **59**, 970.

35 M. W. J. Chase, *NIST-JANAF Thermochemical Tables*, American Institute of Physics, New York, 4th edn, 1998.

36 L. Wang, T. Maxisch and G. Ceder, *Phys. Rev. B: Condens. Matter Mater. Phys.*, 2006, **73**, 195107.

37 S. Grindy, B. Meredig, S. Kirklin, J. E. Saal and C. Wolverton, *Phys. Rev. B: Condens. Matter Mater. Phys.*, 2013, **87**, 075150.

38 Y. Duan, H. Pfeiffer, B. Li, I. C. Romero-Ibarra, D. C. Sorescu, D. R. Luebke and J. W. Halley, *Phys. Chem. Chem. Phys.*, 2013, **15**, 13538.

39 S. Brunauer, P. H. Emmett and E. Teller, *J. Am. Chem. Soc.*, 1938, **60**, 309–319.

40 L. M. Romeo, S. Usón, A. Valero and J. M. Escosa, *Int. J. Greenhouse Gas Control*, 2010, **4**, 647–654.

41 S. Lin, T. Kiga, Y. Wang and K. Nakayama, *Energy Procedia*, 2011, **4**, 356–361.

42 A. Martnez, Y. Lara, P. Lisbona and L. M. Romeo, *Int. J. Greenhouse Gas Control*, 2012, **7**, 74–81.

43 A. Silaban and D. P. Harrison, *Chem. Eng. Commun.*, 1995, **137**, 177–190.

44 M. Aihara, T. Nagai, J. Matsushita, Y. Negishi and H. Ohya, *Appl. Energy*, 2001, **69**, 225–238.

45 Y. Deutsch and L. Heller-Kallai, *Thermochim. Acta*, 1991, **182**, 77–89.

46 P. L. Dulong and A. T. Petit, *Ann. Chim. Phys.*, 1819, **10**, 395–413.

47 K. Nakagawa, *J. Electrochem. Soc.*, 1998, **145**, 1344.

48 J. Ida, R. Xiong and Y. Lin, *Sep. Purif. Technol.*, 2004, **36**, 41–51.

49 M. Kato, S. Yoshikawa and K. Nakagawa, *J. Mater. Sci. Lett.*, 2002, **21**, 485–487.

50 H. Pfeiffer and P. Bosch, *Chem. Mater.*, 2005, **17**, 1704–1710.

51 T. Avalos-Rendon, V. H. Lara and H. Pfeiffer, *Ind. Eng. Chem. Res.*, 2012, **51**, 2622–2630.

52 T. Avalos-Rendon, J. Casa-Madrid and H. Pfeiffer, *J. Phys. Chem. A*, 2009, **113**, 6919–6923.

53 I. Barin and O. Knacke, *Thermochemical Properties of Inorganic Substances*, Springer-Verlag, Berlin, New York, 1973.

54 Q. Wang, J. Luo, Z. Zhong and A. Borgna, *Energy Environ. Sci.*, 2011, **4**, 42–55.

55 D. E. Giammar, R. G. Bruant and C. A. Peters, *Chem. Geol.*, 2005, **217**, 257–276.

56 H. Herzog, *Carbon Sequestration via Mineral Carbonation: Overview and Assessment*, Massachusetts Institute of Technology, Laboratory for Energy and the Environment, Cambridge, Massachusetts, 2002.

57 S. Kwon, M. Fan, H. F. DaCosta and A. G. Russell, *J. Environ. Sci.*, 2011, **23**, 1233–1239.

58 R. L. Martin, B. Smit and M. Haranczyk, *J. Chem. Inf. Model.*, 2012, **52**, 308–318.

59 B. Alcántar-Vázquez, P. R. D. Herrera, A. B. González, Y. Duan and H. Pfeiffer, *Ind. Eng. Chem. Res.*, 2015, **54**, 6884–6892.

60 T. L. Ávalos-Rendón and H. Pfeiffer, *Energy Fuels*, 2012, **26**, 3110–3114.

61 G. Hautier, C. Fischer, V. Ehrlacher, A. Jain and G. Ceder, *Inorg. Chem.*, 2011, **50**, 656–663.

1360 | *Energy Environ. Sci.*, 2016, **9**, 1346–1360

This journal is © The Royal Society of Chemistry 2016